

# Variational Quantum Simulation of the Fokker-Planck Equation applied to Quantum Radiation Reaction

Óscar Amaro <sup>1</sup>†, L. I. Iñigo Gamiz <sup>1</sup>, M. Vranic <sup>1</sup>

<sup>1</sup>GoLP/Instituto de Plasma e Fusão Nuclear, Instituto Superior Técnico, Universidade de Lisboa, Lisbon, Portugal

(Received xx; revised xx; accepted xx)

Near-future experiments with Petawatt class lasers are expected to produce a high flux of gamma-ray photons and electron-positron pairs through Strong Field Quantum Electrodynamical processes.

Simulations of the expected regime of laser-matter interaction are computationally intensive due to the disparity of the spatial and temporal scales and because quantum and classical descriptions need to be accounted for simultaneously (classical for collective effects and quantum for nearly-instantaneous events of hard photon emission and pair creation). A typical configuration for experiments is a scattering of an electron and a laser beam which can be mapped to an equivalent problem with a constant magnetic field.

We study the stochastic cooling of an electron beam in a strong, constant, uniform magnetic field, both its particle distribution functions and their energy momenta. We start by obtaining approximate closed-form analytical solutions to the relevant observables. Then, we apply the quantum-hybrid Variational Quantum Imaginary Time Evolution to the Fokker-Planck equation describing this process and compare it against theory and results from Particle-In-Cell simulations and classical Partial Differential Equation solvers, showing good agreement. This work will be useful as a first step towards quantum simulation of plasma physics scenarios where diffusion processes are important, particularly in strong electromagnetic fields.

## 1. Introduction

Strong-field quantum electrodynamics (SFQED) studies the interaction between matter and intense electromagnetic fields. In recent years, there has been a growing interest in this area due to the availability of high-intensity laser sources, which enable the exploration of novel physical phenomena, with experiments being planned for the near future at: ELI Extreme Light Infrastructure , Apollon Papadopoulos *et al.* (2016), CoReLS Yoon *et al.* (2019), FACET-II ; Meuren *et al.* (2020), LUXE Abramowicz *et al.* (2019, 2021), XCELS , ZEUS , NSF-OPAL , HIBEF , among others.

Many of the proposed experimental setups feature scattering of intense, focused laser pulses with either relativistic electron beams or high-energy photons.

Some experimental evidence for radiation reaction has been observed Cole *et al.* (2018); Poder *et al.* (2018); Los *et al.* (2024). However, for more detailed tests of the models applied in this field, additional theoretical and numerical studies are required to understand the effect of “non-ideal” experimental conditions, such as laser jitter, probe beam emittance, synchronization of the collision, etc. In the future, better control over

† Email address for correspondence: oscar.amaro@tecnico.ulisboa.pt

these parameters will allow precision studies of radiation reaction, that is, the recoil on the charged particles that emit high-energy photons and electron-positron production in the lab, among other processes. These can then be applied in physics models of plasmas in extreme astrophysical environments, such as black holes and pulsar magnetospheres Uzdensky & Rightley (2014); Timokhin (2010); Medin & Lai (2010); Cruz *et al.* (2021); Schoeffler *et al.* (2023).

While current laser technology allows us to test strong-field plasma physics in a “semi-classical” regime, as peak intensity continues to increase, we need to start to explore the fully nonperturbative, quantum dynamics of fermions, high-energy photons and the laser field. This regime is expected to require first-principles simulation techniques, thus putting constraints on the more standard particle-in-cell simulations, even if including Monte-Carlo routines for the quantum processes.

Quantum Computing has the potential to handle the complexity of the many-body-physics dynamics in these extreme plasmas. Recently, the Plasma Physics community has started to adapt standard plasma setups and theory to the quantum algorithmic framework Dodin & Startsev (2021); Joseph *et al.* (2023); Amaro & Cruz (2023). However, the intersection between Plasma Physics, Quantum Field Theory, and Quantum Computing remains unexplored.

In this work, we aim to address some of these questions, first by deriving approximate particle distributions and benchmarking with the particle-in-cell code OSIRIS Fonseca *et al.* (2002), that describes QED effects with Monte-Carlo and has already been tested in this regime Vranic *et al.* (2016), and later by applying a hybrid quantum algorithm to the simulation of a Fokker-Planck equation relevant for SFQED. We choose the simplest possible field configuration, a strong constant magnetic field background, that could be generalised in the future. We start with a relativistic electron beam, which can propagate and lose energy to radiation. We follow the evolution of the electron distribution function over time, accounting for the stochastic nature of the quantum emission.

This manuscript is structured as follows. In section 2, we describe the setup of an electron beam propagating perpendicularly to a strong magnetic field and radiating energy in the form of photons in the so-called semi-classical regime. We introduce the Fokker-Planck equation and derive solutions for the evolution of the distribution function and the first two energy moments, with details in appendix B. In section 3, we describe the quantum variational simulation of the Fokker-Planck equation, the choice of ansatz, and the numerical evolution of the parameters using Variational Quantum Imaginary Time Evolution (VarQITE). Conclusions are given in section 4.

## 2. The Fokker-Planck equation for Quantum Radiation Reaction

In this section, we introduce the main parameters for the physical setup, the Fokker-Planck equation describing the interaction of electrons with an intense magnetic field, and approximate formulas for the first two moments of the electron distribution functions. The importance of quantum effects of relativistic particles in strong fields is controlled by the quantum nonlinearity parameters, which for leptons and photons are given by

$$\chi \equiv \frac{\sqrt{(p_\mu F^{\mu\nu})^2}}{E_S mc}, \quad \chi_\gamma \equiv \frac{\sqrt{(\hbar k_\mu F^{\mu\nu})^2}}{E_S mc} \quad (2.1)$$

where  $m$  is the electron mass,  $c$  is the speed of light in vacuum,  $E_S = m^2 c^3 / (e\hbar) = 1.32 \times 10^{18}$  V/m and  $B_S = E_S / c = 4.41 \times 10^9$  T represent the critical Schwinger electric and magnetic fields,  $e$  is the elementary electric charge,  $\hbar$  is the reduced Planck constant,  $F_{\mu\nu}$

is the electromagnetic field tensor, and  $p_\mu, k_\mu$  are the leptonic and photonic 4-momenta. In the case of a relativistic electron moving perpendicularly to a strong, uniform and constant magnetic field, we have

$$\chi = \gamma B/B_S \quad (2.2)$$

The electron distribution function  $f = dN/d\gamma$ , that is, the number of electrons  $dN$  per interval of energy  $d\gamma$ , evolves through a Fokker-Planck equation describing stochastic energy losses

$$\frac{\partial f(t, \gamma)}{\partial t} = \frac{\partial}{\partial \gamma} \left[ -(Af) + \frac{1}{2} \frac{\partial}{\partial \gamma} (Bf) \right] \quad (2.3)$$

This is the Partial Differential Equation that will be simulated through a quantum algorithm in a later section. The scalar drift and diffusion space-dependent terms can be approximated in the  $\chi \ll 1$  regime as

$$A \sim \frac{2}{3} \frac{\alpha m c^2}{\hbar} \chi^2 = a \gamma^2, \quad B \sim \frac{55}{24\sqrt{3}} \frac{\alpha m c^2}{\hbar} \gamma \chi^3 = \frac{b^2}{2} \gamma^4 \quad (2.4)$$

where  $a \equiv 2\alpha k^2/(3\tau_c)$ ,  $\alpha \equiv e^2/(\hbar c)$  is the fine structure constant, and  $b \equiv \sqrt{55\alpha k^3/(12\sqrt{3}\tau_c)}$ , with Compton time  $\tau_c \equiv \hbar/(mc^2)$ , and normalized magnetic field  $k \equiv B/B_S$  Neitz & Di Piazza (2013); Vranic *et al.* (2016). In general, there are no closed-form solutions for the electron distribution function valid in all regimes of quantum nonlinearity  $\chi$ . Further details on the theory of Quantum Radiation Reaction are presented in appendix B.

### 2.1. Evolution of the electron distribution function

In this section, we use the classical approach of simulating the particle motion coupled with Monte-Carlo to account for the hard-photon emission and quantum radiation reaction. As such, it can describe the evolution of the electron distribution, including the energy loss and quantum stochasticity-induced widening of the spectrum.

In the  $\chi \ll 1$  regime, an initially narrow distribution with energy  $\gamma_0$  retains an approximately Gaussian shape throughout the interaction. Following the approach of Torgrimsson (2024a,b); Blackburn (2024), which is based on a perturbative expansion in  $\chi$ , the mean energy  $\mu = \langle \gamma \rangle = \int \gamma f d\gamma$  and energy spread  $\sigma^2 = \int (\gamma - \mu)^2 f d\gamma$  in a constant magnetic field can be obtained as

$$\frac{\langle \gamma \rangle}{\gamma_0} \sim \frac{1}{1 + 2R_c t/3} + \frac{165\chi_0}{8\sqrt{3}(1 + 2/3R_c t)^2} \log \left( 1 + \frac{2R_c t}{3} \right) \quad (2.5)$$

$$\frac{\sigma^2}{\gamma_0^2} \sim \frac{\sigma_0^2 + 55R_c \chi_0 t / (24\sqrt{3})}{(1 + 2R_c t/3)^4} \quad (2.6)$$

where  $R_c \equiv \alpha b_0 \chi_0$  the classical radiation reaction parameter, and  $b_0 \equiv eB/(m \omega_c)$  is an adimensional normalized magnetic field, and  $\omega_c \equiv eB/(m\gamma_0)$  is the synchrotron frequency. In our simulations, the time is normalized as  $t \rightarrow t \omega_c$ , and the average electron energy and normalized magnetic field are  $\gamma_0 = b_0 = 1800$ . From equation 2.6, the maximum energy spread occurs approximately at  $t \sim 1/(2R_c)$  for  $\sigma_{max} \sim 3^{5/4} \sqrt{55}/64 \gamma_0 \sqrt{\chi_0}$ , which recovers the scaling derived in Vranic *et al.* (2016).

To test the validity of these analytical expressions, we run 1D3V simulations with an

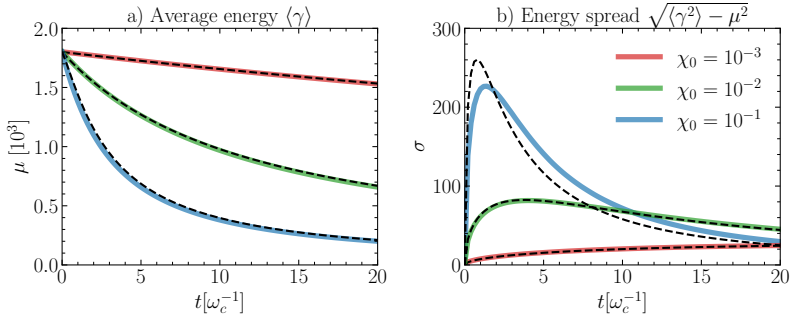


FIGURE 1. a) Average energy and b) spread: OSIRIS simulations (full, color line) vs theory (dashed lines). For the  $\chi_0 = 10^{-1}$  results, the time axis was multiplied by 2 to be visible in the same range as the other values.

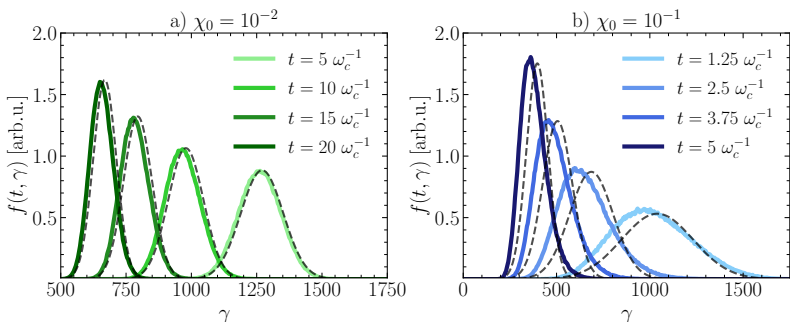


FIGURE 2. Snapshots of the distribution functions, taking the analytical formulas for the mean energy and energy spread (equations (2.5) and (2.6)) for  $\chi_0 = \{10^{-2}, 10^{-1}\}$ . Dashed lines - Gaussian approximation, colored lines - OSIRIS simulation results. For  $\chi_0 = 10^{-1}$  there is a visible deviation from the Gaussian approximation.

electron beam moving perpendicular to the constant, uniform magnetic field vector. The timestep is  $dt = 0.001 \omega_c^{-1}$ , the cell size  $dx = 0.049 c/\omega_c$ , and the normalizing frequencies and external magnetic field values are chosen to enforce  $\chi_0 = \{10^{-3}, 10^{-2}, 10^{-1}\}$ .

In figure 1, we show results from OSIRIS Monte-Carlo simulations for different values of the external magnetic field (different values of initial, average  $\chi_0$ ), and the moments from equations (2.5) and (2.6). The latter expressions capture the simulation results well, with some loss of accuracy for  $\chi_0 = 10^{-1}$ . For the curve  $\chi_0 = 10^{-1}$ , the time axis is scaled ( $\times 2$ ), for better readability.

In figure 2, we show snapshots of Gaussian distribution functions using the parameters  $(\mu, \sigma)$  from equation 2.5, and energy histograms from the OSIRIS Monte-Carlo simulations. Although for  $\chi_0 = 10^{-2}$  there is good agreement with simulation results, it is clear that in the higher  $\chi_0 = 10^{-1}$  regime, the validity of the Gaussian functional approximation is lost, even though the moments  $(\mu, \sigma)$  predicted analytically are close to what was obtained in the simulation. This deviation is due to an increased skewness of the distributions. These results will serve as a “ground truth” for testing the quantum algorithm presented in the following section.

### 3. Variational Quantum Simulation

In this section, we introduce the Variational Quantum Simulation (VQS) method employed in our study.

Quantum Computing holds the potential to revolutionize simulations of complex systems, encompassing both quantum many-body problems and certain classical physics phenomena. The fundamental unit of quantum computation is the qubit, which, unlike a classical bit, can exist in a superposition of states described by  $|\psi\rangle = a_0|0\rangle + a_1|1\rangle$ , where  $a_0$  and  $a_1$  are complex amplitudes satisfying the normalization condition  $|a_0|^2 + |a_1|^2 = 1$  Nielsen & Chuang (2010). When multiple qubits are combined into a register, their joint state can exhibit entanglement — a uniquely quantum mechanical correlation that leads to an exponentially large state space, challenging to simulate efficiently on classical computers.

Currently, quantum computers are in the Noisy Intermediate-Scale Quantum (NISQ) era Preskill (2018), characterized by devices that contain a moderate number of qubits but are susceptible to errors and decoherence. These limitations restrict the depth and complexity of quantum circuits that can be reliably executed, posing significant challenges for implementing algorithms requiring long coherence times and high gate fidelities.

To address these challenges, Variational Quantum Circuits (VQCs) have emerged as a promising approach suitable for NISQ devices. VQCs are hybrid quantum-classical algorithms that employ parameterized quantum circuits optimized using classical optimization routines to minimize a cost function, typically the expectation value of an observable. This method reduces the required circuit depth by offloading part of the computational workload to classical processors, making it more practical for current quantum hardware. Variational quantum algorithms have found applications across various fields, including Quantum Chemistry, Material Science, Biology and others Peruzzo *et al.* (2014). By carefully designing the variational circuits and selecting appropriate ansätze, VQCs leverage the expressive power of quantum systems while operating within the practical constraints of NISQ devices. Extracting meaningful information from the exponentially large quantum state space necessitates meticulous selection and measurement of observables, as quantum measurements yield probabilistic outcomes that collapse the superposed state. The variational approach thus provides a flexible and adaptive framework for quantum simulation, contributing significantly to the advancement of quantum computing applications in science and engineering.

In Plasma Physics, several phenomena of interest are intrinsically dissipative. Since dissipation is an irreversible process, this is challenging to model on quantum computers. In Engel *et al.* (2019), the authors studied Landau damping on a quantum framework using a linearized version of the Vlasov equation. Despite the name “damping”, the energy of the system is not lost but rather transferred from the electric field to the particle distribution function in a reversible/unitary manner. In Vissers & Bouten (2019) a “quantum stochastic” process of a laser driven two-level atom interacting with an Electromagnetic field is studied. However, a procedure to generalize beyond two-level systems is not provided. In Kubo *et al.* (2021), a Partial/Stochastic Differential Equation (PDE/SDE) solver of the Fokker-Planck equation in the form of an Itô-process is proposed in a Quantum Variational framework. This approach was then generalized in Alghassi *et al.* (2022) through the Feynman-Kac formula, which unifies the heat, Schrödinger, Black-Scholes, Hamilton-Jacobi, and Fokker-Planck equations under this formalism.

The expressibility of variational quantum circuits is one of the most important figures of merit in the field of VQS. It is defined as the ability of the variational quantum circuit

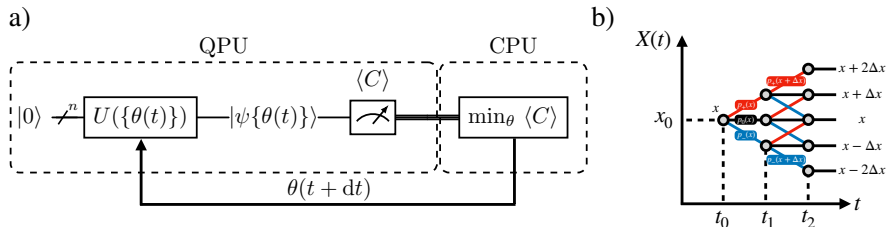


FIGURE 3. a) Variational quantum algorithm. From the Quantum Processing Unit (QPU) we measure a cost function, from which the variational parameters are optimized in the CPU. b) Finite Difference “trinomial model” exemplifying the locality of the Fokker-Planck operator (adapted from Kubo *et al.* (2021)).

to produce a variety of quantum wavefunctions — the higher this value, the larger the fraction of the Hilbert space accessible through the circuit. This metric has been studied in detail, and heuristics on which architectures one can reach higher expressibility have been discussed Sim *et al.* (2019). However, few proofs or universal rules have been derived so far. In the case of Kubo *et al.* (2021), the authors suggest using an ansatz with only  $R_Y$  and CNOT quantum gates, which permits only real-valued amplitudes of the wavefunction, but it also allows for negative values. In Dasgupta & Paine (2022), the authors suggest an architecture to enforce even-symmetry of the real-valued wavefunction around the middle of the computational basis representation. In Endo *et al.* (2020), the motivation for using compact variational circuits is based on the intuition that the dynamics of the physical system only span low energy states and therefore is limited to a small portion of the entire Hilbert space.

In this work, we consider wave/distribution functions that are well localized in space but can have a mean position/energy which can be off-centred, that is, not located at the middle of the computational basis  $|01\dots 1\rangle, |10\dots 0\rangle$ . For this, we use a quantum circuit which simulates the advection equation based on the finite differences operator as presented in Sato *et al.* (2024). This operation can be used to shift the entire wavefunction, which allows the exploration of a larger space of states.

In figure 3, we show the hybrid quantum optimization loop. First, at a time-step  $t$ , a quantum wavefunction is produced by the quantum circuit, where some of the quantum unitary operations are parametrized by values  $\theta(t)$ . Then, a cost function / observable  $\langle C \rangle$  is measured from the quantum circuit and minimized/updated through an algorithm run on a classical device. The new parameters are then fed-back to the quantum circuit to produce the wavefunction for the next time step  $\theta(t + dt)$ . The Finite-Difference approximation to the Fokker-Planck operator is of the trinomial type, where any grid cell at any time step is only influenced by its two close neighboring cells. Higher-order Finite-Difference schemes are possible to apply but require more complex algorithms.

### 3.1. Variational ansatz

In figure 4, we show the ansatz used in this work. In the first variational block (blue), we produce a real-valued wavefunction using parameters  $\theta$  and gates CNOT –  $R_Y$  in a ring structure (the qubit  $n - 1$  connects with the first qubit). This block can be repeated to increase the expressibility of the ansatz. The second block (red) consists of enforcing even-symmetry on the wavefunction; that is, the amplitudes have a mirror symmetry around half of the computational basis  $\psi_{0111} = \psi_{1000}, \psi_{0000} = \psi_{1111}$ . If, instead, we apply an angle  $-\pi/2$  on the  $R_Y$  gate acting on the last qubit, then the wavefunction

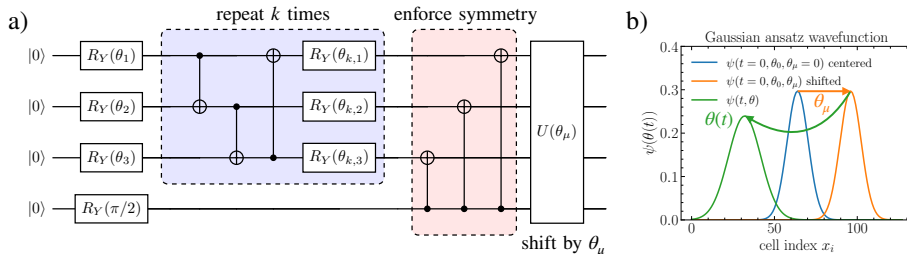


FIGURE 4. a) Variational ansatz used in this work. Only 4 qubits are shown for simplicity. The blue box represents a variational block that can be repeated. The red box represents the enforcing of even-symmetry on the wavefunction. In the last step, the advection operator is applied. b) Sketch of the typical evolution of the wavefunction.

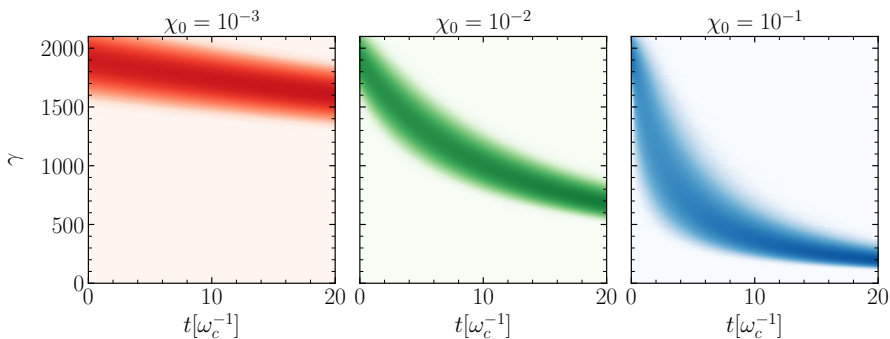


FIGURE 5. Evolution of electron distribution functions from OSIRIS simulations for different initial average  $\chi_0$  values and  $\sigma_0 = 90$ .

becomes odd instead of even-symmetric. At  $t = 0$ , we fit these parameters so that the wavefunction has an approximate Gaussian shape with a prescribed standard deviation  $\sigma$ . In this way, the parameters  $\theta$  are implicit functions of  $\sigma$ .

In the final step of the quantum circuit, we apply the advection operator  $e^{-i\theta_\mu \partial_x}$ , which is a unitary operation, and which translates the entire wavefunction by some quantity  $\theta_\mu$ . In Sato *et al.* (2024), the authors provide a quantum circuit for the Finite-Difference version of the 1st order of  $\partial_x \sim (s_+ - s_-)/2$ , where  $s_+ = s_-^\dagger$  is the operator that shifts the wavefunction one cell to the right (left) with a periodic boundary condition. Here, we use the 2nd order of this Finite-Difference operator to enforce higher fidelity of the translation.

### 3.2. Variational Quantum Simulation of the Fokker-Planck equation

In figure 5, we show the complete evolution of the distribution functions for  $\mu_0 = 1800$ ,  $\sigma_0 = 90$  from OSIRIS Monte-Carlo simulations, following the same setup parameters as in Niel *et al.* (2018), which we take as being the “ground-truth” benchmark. In these simulations, the electrons can be seen to cool down quicker for higher  $\chi_0$ , and the distribution functions occupy different fractions of the energy domain throughout the evolution, thus having different requirements on the resolution for the energy grid.

The VQS algorithm maps the dynamics of the quantum state, equation 2.3, to those of the variational parameters  $\theta(t)$  of the ansatz. The mapping is performed using McLachlan’s variational principle (MVP) McLachlan (1964); Endo *et al.* (2020). Using the same notation as in Kubo *et al.* (2021), the unitary quantum circuit produces a wavefunction

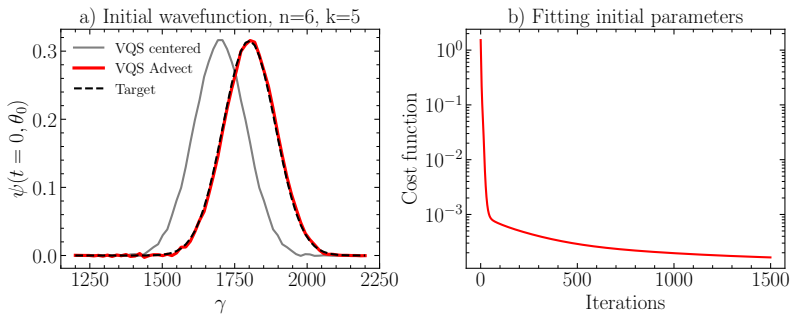


FIGURE 6. Fitting of the initial wavefunction for  $\chi_0 = 10^{-3}$ ,  $n = 6$  qubits and  $k = 5$  layers of variational parameters. Left: a centered wavefunction is obtained through fitting the variational parameters. Right: evolution of the cost function as the optimizer converges on a good approximation of the target wavefunction.

$|v\{\boldsymbol{\theta}(t)\}\rangle$ . However, diffusive processes generally do not preserve the  $L_2$  norm, that is,  $\partial_t \int |v|^2 dx \neq 0$ . Therefore, it is useful to define an overall variational wavefunction  $|\tilde{v}\{\boldsymbol{\theta}(t)\}\rangle = \alpha(t) |v\{\boldsymbol{\theta}(t)\}\rangle$  where  $\alpha(t)$  is a (classical) normalization parameter. If the temporal resolution is sufficiently high and the ansatz sufficiently expressive, the MVP method evolves the variational parameters such that the correct dynamics are enforced through

$$\min_{\boldsymbol{\theta}(t)} \left\| \frac{d}{dt} |\tilde{v}\{\boldsymbol{\theta}(t)\}\rangle - \hat{L} |\tilde{v}\{\boldsymbol{\theta}(t)\}\rangle \right\| \quad (3.1)$$

where  $\hat{L}$  is a linear operator that generates the evolution of the system. At each time step, the following matrix equation needs to be solved

$$M_{k,j} \dot{\theta}_j = V_k \quad (3.2)$$

where

$$M_{k,j} \equiv \text{Re} \left( \frac{\partial \langle \tilde{v}\{\boldsymbol{\theta}(t)\} | \partial \tilde{v}\{\boldsymbol{\theta}(t)\} \rangle}{\partial \theta_k} \frac{\partial \tilde{v}\{\boldsymbol{\theta}(t)\}}{\partial \theta_j} \right), \quad V_k \equiv \text{Re} \left( \frac{\partial \langle \tilde{v}\{\boldsymbol{\theta}(t)\} | \hat{L} \tilde{v}\{\boldsymbol{\theta}(t)\} \rangle}{\partial \theta_k} \right) \quad (3.3)$$

are quantities that can be obtained efficiently through dedicated quantum circuits. One advantage of this method, if run on a quantum device, is that one does not need to have access to the full amplitudes of the wavefunction. Instead, only the variational parameters need to be tracked, and their evolution is obtained through efficient measurement of a few observables. Whereas the  $M_{k,j}$  only depend on the chosen ansatz, the  $V_k$  elements depend on both the ansatz and the particular Fokker-Planck equation operators (in this case equation 2.3). In this work, we classically simulate the retrieval of these quantities through numerical differentiation and integration of the wavefunction using *Numpy Harris et al.* (2020).

As previously explained, we first optimize the parameters (except for  $\theta_\mu$ , which we keep fixed) using a cost function  $C = \|\psi(\boldsymbol{\theta}) - \psi_{target}\|^2$ . We choose a number of iteration steps such that the cost function has decreased significantly and converged such that the quantum variational ansatz produces the centered target distribution (see figure 6). After this, we apply the advection step by changing the parameter  $\theta_\mu$  to match the initial mean value of the distribution on the energy grid.

In figure 7, we show the VarQITE simulation of the distribution function for  $\chi_0 =$



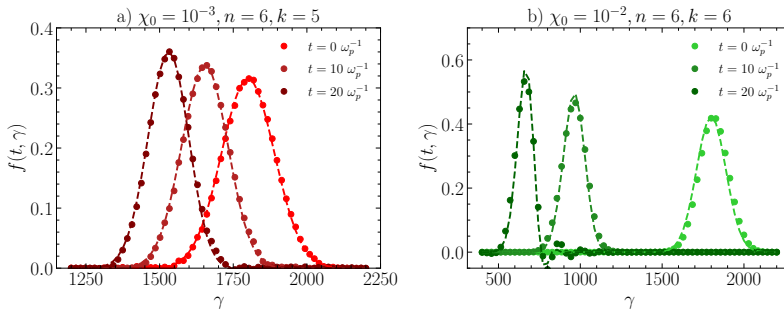


FIGURE 7. Evolution of electron distribution functions for  $\chi_0 = 10^{-3}, 10^{-2}$ . Dashed line - PDE solver, Circles - VarQITE. In both cases,  $n = 6$  qubits, while the number of layers is  $k = 5, 6$  for the two setups. a) simulation results for  $\chi = 10^{-3}$ . b) simulation results for  $\chi = 10^{-2}$

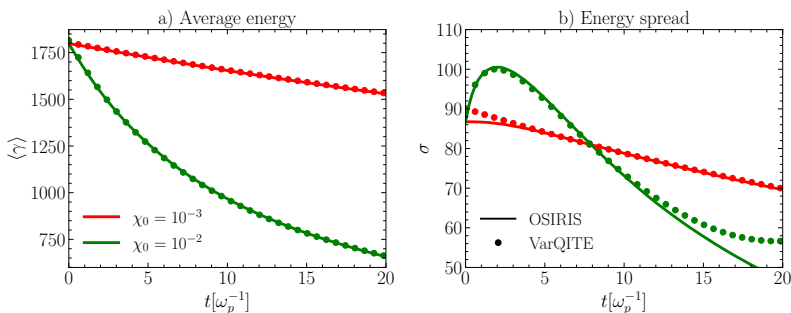


FIGURE 8. Evolution of the moments of the distribution functions obtained through VarQITE (circles) and compared against OSIRIS (lines). a) the first moment (mean), b) second moment (spread).

$\{10^{-3}, 10^{-2}\}$ , and results from solving the PDE with a classical algorithm. We thus show the capability of VarQITE to simulate classical distribution functions relevant to plasma physics.

In figure 8, we show the evolution of the first two moments of the distribution functions. There is a general agreement of the quantum circuit results with the OSIRIS simulations. There is a small deviation due to finite grid resolution, which can be resolved by increasing the number of qubits.

In figure 9, we show the evolution of all the 27 variational parameters for the  $\chi_0 = 10^{-3}$  case. The trajectories are smooth, and some parameters have minimal deviations, which suggests that the ansatz is over-parametrized and can be made more efficient. Figure 9 b) shows the values of the mean energy computed from the wavefunction produced by the quantum variational ansatz against the variational parameter responsible for the translation  $e^{-i\theta_\mu \partial_x}$ , where a linear scaling between the two is visible.

### 3.3. A note on the extraction of moments of the distribution function

The global translation of the wavefunction is correlated with the average energy through a simple rescaling. Therefore, we would not need to measure the mean energy of the wavefunction because we could simply read this value from one of the variational parameters. This is only allowed because of our choice of a translated, even-symmetric wavefunction and would not be viable if the ansatz allowed for skewed distributions.

The average and variance of the energy can be measured efficiently ( $n$   $Z_i$ , plus  $n$  and

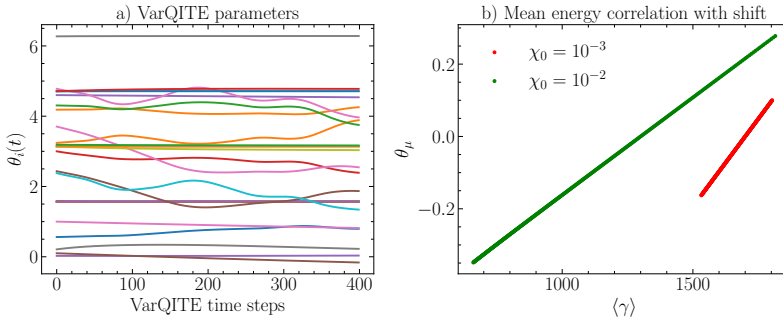


FIGURE 9. a) The evolution of variational parameters for  $\chi_0 = 10^{-3}$ , b) the linear correlation between average energy from the wavefunction and the parameter of the wavefunction translation.

$2n$   $Z_i Z_j$  gates, respectively), with a Pauli-string decomposition of the observables:

$$\hat{x} = \frac{1}{2}(2^n - 1)I - \frac{1}{2} \sum_{i=0}^{n-1} 2^{n-i-1} Z_i \quad (3.4)$$

$$\hat{x}^2 = \left( a^2 + \sum_{i=0}^{n-1} b_i^2 \right) I + 2a \sum_{i=0}^{n-1} b_i Z_i + 2 \sum_{0 \leq i < j \leq n-1} b_i b_j Z_i Z_j \quad (3.5)$$

with  $a = \frac{1}{2}(2^n - 1)$ ,  $b_i = -\frac{1}{2} \times 2^{n-i-1}$ , and  $Z_i$  is the Pauli- $Z$  gate applied to qubit  $i$ . The commutation relation between the individual terms can be used to make the measurement more efficient, and the results of  $\langle x \rangle = \langle \psi | \hat{x} | \psi \rangle$ ,  $\langle x^2 \rangle = \langle \psi | \hat{x}^2 | \psi \rangle$  can then be linearly rescaled to be compatible with the wavefunction domain in energy  $\gamma$ .

## 4. Conclusions

In this work, we present a quantum-hybrid algorithm approach to Quantum Radiation Reaction, providing similar results when benchmarked against the particle-in-cell (PIC) code OSIRIS. We have simulated the Fokker-Planck equation describing the stochastic cooling of an electron population in a strong magnetic field using the Variational Quantum Imaginary Time Evolution algorithm (VarQITE), showing good agreement with the results from PIC. We have developed a new variational ansatz that mimics a Gaussian trial-function, capturing the first and second moments of the distribution functions while requiring fewer parameters than more general variational ansätze. We have also derived closed-form analytical results for moments of the energy distribution functions, their entropy and autocorrelation functions.

Future steps will include extending this approach to other Fokker-Planck equations of interest (for example, the Kompaneets equation or laser cooling of trapped atoms), to the full Boltzmann equation (nonlocal operator), and to represent the quantum system not as a classical distribution function but as a Fock-state Hidalgo & Draper (2024), where the dynamics would be naturally unitary. Additionally, using specialized circuits for loading specific distribution functions as part of the variational ansatz (Gaussian, Uniform, Chi-squared) could lead to a reduced number and more interpretable parameters, which would speedup the VarQITE algorithm and possibly mitigate the barren-plateau problem.

Our work can contribute to further development of both classical diffusive plasma physics and to simulate the fully quantum nature of plasma interactions, namely the transition from semi-classical to nonperturbative SFQED regimes.

## 5. Data and Code availability statement

The data that support the findings of this study are openly available at the following URL/DOI: <https://github.com/OsAmaro/QuantumFokkerPlanck>. The repository includes notebooks explaining the classical PDE solver, the VarQITE approach, the analytical models and input decks for OSIRIS simulations.

## 6. Acknowledgments

The authors thank the following people for fruitful discussions / proofreading parts of the manuscript: Mr. José Mariano on Monte-Carlo sampling, Mr. Lucas Ansia on classical simulation of the Fokker-Planck equation, Mr. Bernardo Barbosa on Quantum Radiation Reaction in SFQED, Mr. Pablo Bilbao on plasma dynamics in strong magnetic fields, Mr. Gabriel Almeida on expressibility and complexity of variational quantum circuits, Mr. Anthony Gandon on efficient Pauli-String decomposition of Hamiltonians for variational quantum circuits, Mr. Efstratios Koukoutsis on Lindbladian/dissipative quantum simulations, and Mr. Diogo Cruz on quantum algorithms for PDE solvers.

This work was supported by the Portuguese Science Foundation (FCT) Grants No. PTDC/FIS-PLA/3800/2021, UI/BD/153735/2022. This work has been carried out within the framework of the EUROfusion Consortium, funded by the European Union via the Euratom Research and Training Programme (Grant Agreement No 101052200 — EUROfusion). Views and opinions expressed are however those of the authors only and do not necessarily reflect those of the European Union or the European Commission. Neither the European Union nor the European Commission can be held responsible for them.

Simulations were performed at the IST cluster (Lisbon, Portugal). We have used the quantum frameworks Qiskit Javadi-Abhari *et al.* (2024) and PennyLane Bergholm *et al.* (2022).

## Appendix A. Applying the Variational Principle to the Heat equation

In this appendix, we provide a step-by-step application of McLachlan’s Variational Principle (MVP) to the simplest diffusive PDE, the heat equation. Similar to the Classical Variational Principle used in Quantum Mechanics to obtain approximate Ground-States of a system, the MVP for imaginary or real-time evolution is useful both numerically and analytically.

The 1D homogeneous heat equation

$$\partial_t u = k \partial_{xx} u \tag{A1}$$

with thermal diffusivity coefficient  $k$ , admits a kernel solution (when  $u(t=0, x) = \delta(x)$ )

$$u(t, x) = \frac{1}{\sqrt{4\pi kt}} \exp\left(-\frac{x^2}{4kt}\right) \tag{A2}$$

from which analytical solutions to more general initial conditions can be constructed.

This suggests using an ansatz

$$v(A, \sigma) = A \exp\left(-\frac{x^2}{2\sigma^2}\right), \quad \partial_t v = \hat{L}_H v \tag{A3}$$

with  $\hat{L}_H$  the linear operator generating the evolution of the system (in this case, it is

the Laplacian  $\partial_{xx}$ ), and variational parameters  $\theta_i(t) = (A(t), \sigma(t))$ , for the analytical solution of the MVP. We take the thermal diffusivity to be  $k = 1$  for simplicity. Since this function is  $L_1$ -normalized (that is,  $\int v dx = 1$ ), the normalization  $A$  will be correlated and a function of the parameter  $\sigma$ .

The following derivatives and integrals are used in the calculations

$$\begin{aligned} \partial_A v &= A^{-1} v, \quad \partial_\sigma v = x^2 \sigma^{-3} v, \quad \partial_{xx} v = v (x^2 - \sigma^2) \sigma^{-4} \\ \int v dx &= A\sqrt{2\pi}\sigma, \quad \int v^2 dx = A^2\sqrt{\pi}\sigma \\ \int x^2 v^2 dx &= A^2\sqrt{\pi}\sigma^3/2, \quad \int x^4 v^2 dx = 3A^2\sqrt{\pi}\sigma^5/4 \end{aligned} \tag{A 4}$$

From the MVP equations 3.3, we need to compute the matrix elements  $\int (\partial_k v)(\partial_j v) dx$ , which require either the  $\int v^2 dx$  or  $\int x^2 v^2 dx$  integrals. We obtain

$$M_{A,A} = \sqrt{\pi}\sigma, \quad M_{A,\sigma} = M_{\sigma,A} = \sqrt{\pi}A/2, \quad M_{\sigma,\sigma} = 3\sqrt{\pi}A^2/(4\sigma),$$

For the column vector, we need to compute  $\int (\partial_k v)(\hat{L}_H v) dx$ . We obtain

$$V_A = -A\sqrt{\pi}/(2\sigma), \quad V_\sigma = A^2\sqrt{\pi}/(4\sigma^2)$$

We now need to solve the matrix equation  $M_{k,j}\dot{\theta}_j = V_k$ . Factors of  $\sqrt{\pi}$  will cancel out.

$$\begin{bmatrix} \sigma & A/2 \\ A/2 & 3A^2/(4\sigma) \end{bmatrix} \begin{bmatrix} \dot{A} \\ \dot{\sigma} \end{bmatrix} = V_k \leftrightarrow \begin{bmatrix} \dot{A} \\ \dot{\sigma} \end{bmatrix} = \begin{bmatrix} 3/(2\sigma) & -1/A \\ -1/A & 2\sigma/A^2 \end{bmatrix} \begin{bmatrix} -A/(2\sigma) \\ A^2/(4\sigma^2) \end{bmatrix} = \begin{bmatrix} -A/\sigma^2 \\ 1/\sigma \end{bmatrix} \tag{A 5}$$

where we explicitly computed the matrix inverse of  $M_{k,j}$ . The second equation (for  $\sigma$ ) is separable. We can then replace  $\sigma(t)$  in the first equation to obtain the amplitude  $A(t)$ . The parameters thus become

$$\sigma(t) = \sqrt{2t + \sigma_0^2}, \quad A(t) = A_0\sigma_0/\sqrt{2t + \sigma_0^2} \tag{A 6}$$

where  $\sigma_0, A_0$  are the initial spread and amplitude, respectively. This is precisely the exact analytical solution A 2. In figure 10, we show a comparison between a standard PDE solver solution of the heat equation, a numerical solution of the MVP equations using the ansatz A 3 (without a quantum circuit), and the analytical solution A 6. The numerical grid had  $2^6$  cells, the number of timesteps was 200 for a maximum simulation time of 40, and a small initial spread of the distribution function  $\sigma_0 = 0.01$ .

## Appendix B. The Fokker-Planck equation

### B.1. Review of theoretical study of Radiation Reaction

In this section we review past works on radiation reaction, introduce the main parameters that describe the interaction of electrons with an intense magnetic field, and derive analytical solutions for some observables of interest.

In the past decades, the theoretical modelling of electron radiation losses in intense fields has been extensively studied. In Shen & White (1972), authors derive the transport partial differential equation (PDE) for electrons in a constant uniform magnetic field. Analytical results of multi-photon scattering of electrons in periodic structures (e.g.

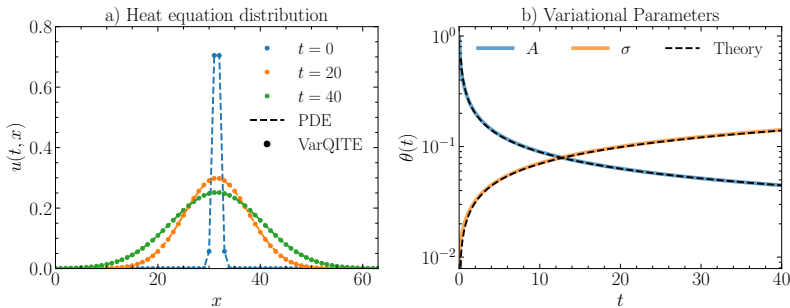


FIGURE 10. Numerical solution of the 1D Heat equation. a) Snapshots of the distribution  $u(t, x)$  from a PDE solver and numerical evolution of a Gaussian ansatz in the MVP. b) Evolution of the variational parameters: color - numerical MVP, dashed - analytical solution to the MVP equations A 6.

oriented-crystals) have been derived in Khokonov (2004); Bondarenco (2014), however without simple explicit closed-form expressions for the observables, nor immediate application in electron-laser scattering. In Lobet *et al.* (2016), the coupled dynamics of photons and leptons, including radiation reaction and pair production in a constant magnetic field, are studied numerically. In Vranic *et al.* (2016); Ridgers *et al.* (2017); Niel *et al.* (2018) the authors derive the Ordinary Differential Equations (ODEs) for the first two moments of the energy distributions of electrons interacting with a laser pulse, but don't present their corresponding closed-form explicit solutions. In Niel *et al.* (2018), the authors show connections between the different regimes of radiation reaction and the corresponding particle trajectories and stochastic PDEs. In Artemenko *et al.* (2019), the electron transport PDE is solved numerically for different magnetic field values using the ‘‘Global Constant Field Approximation’’ to map between a constant magnetic field setup and a laser pulse with a finite duration envelope. In Jirka *et al.* (2021), the authors derive the average energy decay in a pulsed Plane Wave laser in the highly ‘‘nonlinear quantum’’ high  $\chi$  regime (the quantum nonlinear parameter,  $\chi$ , is defined in section 2).

More recently, some papers have contributed with new analytical results for the study of classical (CRR) and quantum (QRR) radiation reaction regimes. In Bilbao & Silva (2023), authors derive analytically the evolution of an electron momentum ‘‘ring distribution’’ in a maser setup, relevant for astrophysical plasma scenarios. The formulas are derived in the CRR regime using the ‘‘method of lines’’ technique but appear to hold even for  $\chi \sim 0.1$ , and suggest that this class of ring distributions is a ‘‘global attractor’’. In Zhang *et al.* (2023), the authors derive approximate analytical formulas for the evolution of a lepton distribution function in a constant magnetic field during multiphoton scattering in the QRR  $\chi < 1$  regime. The authors identify and analytically characterise the ‘‘quantum peak splitting’’, which occurs when an initially peaked distribution function evolves into a doubly peaked distribution. In Bulanov *et al.* (2024), the authors derive CRR closed-form expressions for distribution functions for a set of initial conditions of interest, again using the ‘‘method of lines’’, and find an equilibrium (time-independent) solution for the QRR Fokker-Planck equation of an electron beam in a LWFA setup. In Kostyukov *et al.* (2023), the authors derive short-time evolution expressions for the electron wave packet in a strong EM field, including the expectation value of the electron spin. The approach relies on Volkov functions and the Dyson-Schwinger equation and naturally leads to the damping (radiation reaction) of the wave packet. In Torgrimsson (2024a,b) the author derives explicit analytical time-dependent electron distribution functions in momentum and spin through resummation techniques. Following a similar approach, in Blackburn

(2024), the author derives explicit analytical QRR formulas for the final electron mean energy and spread as functions of initial electron energy, laser  $a_0$  and pulse duration. These expressions are derived in the low  $\chi$  regime but remain approximately valid for a larger range of parameters.

### B.2. Regimes of Radiation Reaction

Here we follow the notation of Vranic *et al.* (2016). When  $\chi \ll 1$ , the equation for energy loss can be derived from the Landau-Lifshitz equation, leading to

$$\frac{d\gamma}{dt} = -c_{rr} \gamma^2 \quad (\text{B1})$$

with  $c_{rr} \equiv 2 \omega_c e^2 b_0^2 / (3mc^3)$  a constant defining the effect of Classical Radiation Reaction. In the setup considered, 3 physical parameters completely describe the dynamics: the initial electron energy  $\gamma_0$ , the external magnetic field  $B$ , and the evolution time  $t$ . The solution for the energy is

$$\gamma_e(t) \sim \gamma_0 / (1 + c_{rr} t \gamma_0) \quad (\text{B2})$$

This scaling for the average energy can be corrected in the  $\chi \lesssim 1$  regime.

From a distribution point of view, the relativistic Vlasov equation for the electron distribution function  $f$  is modified. Radiation Reaction no longer preserves phase-space volume, corresponding to the operator on the RHS of the equation

$$\frac{df(t, \vec{x}, \vec{p})}{dt} = \frac{\partial f}{\partial t} + v \cdot \nabla_x f + F \cdot \nabla_p f = \mathcal{C}[f_e] \quad (\text{B3})$$

where  $\mathcal{C}$  is a collision operator whose form depends on the model/regime of radiation reaction considering Niel *et al.* (2018). In our simplified setup, the coordinate gradient and the force terms vanish, so the only term of interest is the collision operator.

For higher values of  $\chi$ , the emission of photons becomes stochastic, in general leading to a spread in energy. Conceptually, the electrons can be thought of as being slightly scattered through a cloud of photons of the field, where each photon has an energy much lower than the electron's.

The probability of emission of a photon with  $\chi_\gamma$  by an electron with  $\chi$  per unit time, also known as the nonlinear Compton Scattering (nCS) differential cross section/rate, is

$$\frac{d^2 N_\gamma}{dt d\chi_\gamma}(\chi, \chi_\gamma) = \frac{\alpha mc^2}{\sqrt{3}\pi \hbar \gamma \chi} \left[ \left( 1 - \xi + \frac{1}{1 - \xi} \right) K_{2/3}(\tilde{\chi}) - \int_{\tilde{\chi}}^{\infty} K_{1/3}(x) dx \right] \quad (\text{B4})$$

with  $\xi \equiv \chi/\chi_\gamma$ ,  $\tilde{\chi} \equiv 2\xi/(3\chi(1 - \xi))$ , and  $K_n$  is the modified Bessel function of second kind Abramowitz & Stegun (1964). This rate in  $\chi_\gamma$  can be mapped to a rate in particle energy  $d^2 N_\gamma / dt d\gamma_\gamma(\gamma, \gamma_\gamma)$ .

The Fokker-Planck equation (FP) can be seen as an extension of the standard Vlasov equation to kinetically and stochastically model collisions between plasma species and laser-plasma interaction. An important application is simulating the energy loss of an electron beam as it interacts with electromagnetic fields Neitz & Di Piazza (2013); Vranic *et al.* (2016). In this case, the particle distribution evolves through

$$\frac{\partial f(t, \vec{p})}{\partial t} = \frac{\partial}{\partial p_l} \left[ -\mathcal{A}_l f + \frac{1}{2} \frac{\partial}{\partial p_k} (\mathcal{B}_{lk} f) \right] \quad (\text{B5})$$

with  $\mathcal{A}_l \equiv \int q_l w(\vec{p}, \vec{q}) d^3 \vec{q}$ ,  $\mathcal{B}_{lk} \equiv \int q_l q_k w(\vec{p}, \vec{q}) d^3 \vec{q}$ , the drift and diffusion coefficients

respectively, and  $w(\vec{p}, \vec{q}) d^3\vec{p}$  is the probability per unit time of momentum change of the electron  $\vec{p} \rightarrow \vec{p} - \vec{q}$ , with  $\vec{q}$  the momentum of the photon, and where Einstein index contraction was assumed.

In the co-linear approximation of radiation emission,  $\chi_\gamma/\chi \sim \hbar k/(\gamma mc)$ , this problem becomes essentially 1D, with drift and diffusion coefficients

$$\mathcal{A} \equiv \frac{\gamma mc}{\chi} \int_0^\chi \chi_\gamma \frac{d^2 N_\gamma}{dt d\chi_\gamma} d\chi_\gamma, \quad \mathcal{B} \equiv \frac{(\gamma mc)^2}{\chi^2} \int_0^\chi \chi_\gamma^2 \frac{d^2 N_\gamma}{dt d\chi_\gamma} d\chi_\gamma \quad (\text{B6})$$

In the regime of  $\chi \ll 1$ , the  $\mathcal{A}$  and  $\mathcal{B}$  coefficients have polynomial approximations Vranic *et al.* (2016)

$$\mathcal{A} \sim \frac{2}{3} \frac{\alpha m^2 c^3}{\hbar} \chi^2 \propto \gamma^2, \quad \mathcal{B} \sim \frac{55}{24\sqrt{3}} \frac{\alpha m^3 c^4}{\hbar} \gamma \chi^3 \propto \gamma^4 \quad (\text{B7})$$

The Fokker-Planck equation is sparse (only 2 local, differential operators), while the Boltzmann equation is nonlocal, and its corresponding Hamiltonian evolution matrix is dense. Consequently, both numerical (either a PDE solver or Monte-Carlo sampling) and analytical solutions of the latter equation are often more challenging than for the former.

### B.3. Entropy and Autocorrelation

Having derived the evolution of the spread 2.6, and assuming a Gaussian functional form of the distribution function, the Shannon entropy of the electron beam evolves as  $S(t) = -\int f \log(f) d\gamma \sim \log(\sigma(t)) + c^{te}$  up to an additive constant (which we choose such that the simulation and theory curves match at late times). Since this is a monotone function of the spread, it has the same qualitative behavior and peaks at  $\log(\sigma_{\max})$ . From a physics point-of-view, the entropy changes due to a competition between the drift and diffusion processes. At late times, the entropy of the electrons decreases, which can be interpreted as a transfer of entropy to the radiation that is being emitted.

One can also compute an approximate auto-correlation function from the classical solution  $\gamma_c(t) \sim \gamma_0/(1 + 2R_c t/3)$  as

$$g(\tau) \equiv \frac{\langle \gamma(t)\gamma(t+\tau) \rangle}{\langle \gamma^2(t) \rangle} = \int_0^\infty \frac{1}{(1 + 2R_c t/3)(1 + 2R_c(t+\tau)/3)} dt \propto \frac{\log(1 + 2R_c \tau/3)}{2R_c \tau/3} \quad (\text{B8})$$

where normalization  $g(0) = 1$  is enforced. This quantifies how correlated two electron trajectories are on average if measured with a time delay of  $\tau$ . Using instead the 2nd order expansion for the average energy (that is, the full equation 2.5) leads to a more accurate closed-form solution, albeit with more terms (not shown here). Considering the stochastic component of the trajectories would require computing expectation values of nonlinear functions of Wiener processes  $W(t), W(t + \tau)$ . The solution to the Fokker-Planck equation  $f(t, \gamma)$  does not give us information on the auto-correlation directly, and a marginal distribution  $f(t_1, \gamma_1; t_2, \gamma_2)$  would have to be obtained.

In figure 11, we show the comparison between these two quantities  $S(t), g(\tau)$  from OSIRIS simulations computed from distribution histograms and individual particle trajectories, and the approximate analytical results. Again, for  $\chi_0 = 10^{-1}$  (blue curve), the  $t$ -axis is again multiplied by a factor of 2 to have the same range as the other curves.

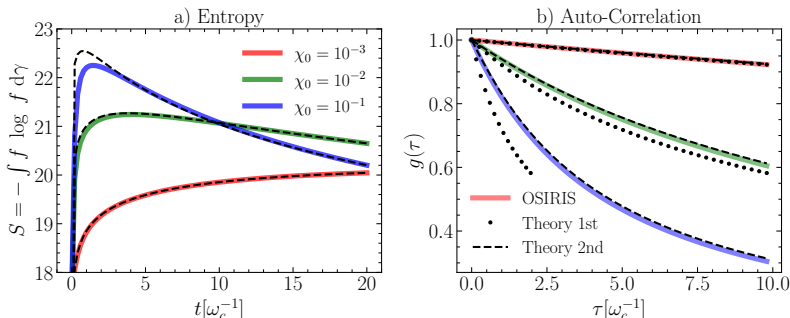


FIGURE 11. a) The evolution of the distribution function entropy, b) auto-correlation function, where dotted lines represent equation B 8 and dashed lines are the result of using 2.5 in  $g(\tau)$ . In both figures, lines in color represent results from OSIRIS simulations.

#### B.4. McLachlan's Variational Principle approach

Here, we apply the technique described in A to the Fokker-Planck equation. Since the number of particles ( $L_1$  norm) is conserved and we are mostly interested in the first moments of the distribution function  $\mu = \int \gamma f d\gamma$ ,  $\sigma^2 = \int (\gamma - \mu)^2 f d\gamma$ , we enforce this into the ansatz

$$v(\mu, \sigma) = \frac{1}{\sqrt{2\pi}\sigma^2} \exp\left(-\frac{(\gamma - \mu)^2}{2\sigma^2}\right), \quad \partial_t v = \hat{L}_{FP} v = -\partial_\gamma(a\gamma^2 v) + 0.5 \partial_{\gamma\gamma}(b\gamma^4 v) \quad (\text{B 9})$$

with  $\hat{L}_{FP}$  the linear operator generating the dynamics, and variational parameters  $\theta_i(t) = (\mu(t), \sigma(t))$ , for the analytical solution of the MVP. We could have used an ansatz with the amplitude  $A(t)$ , which would have led to a 3x3 matrix system of equations.

The following derivatives will be used in the following calculations

$$\frac{\partial_\mu v}{v} = \frac{\gamma - \mu}{\sigma^2}, \quad \frac{\partial_\sigma v}{v} = \frac{(\gamma - \mu)^2 - \sigma^2}{\sigma^3} \quad (\text{B 10})$$

From the MVP equations 3.3, we need to compute the matrix elements  $\int (\partial_k v)(\partial_j v) d\gamma$ , which require either the  $\int (\gamma - \mu)^2 v^2 d\gamma$  or the  $\int (\gamma - \mu)^4 v^2 d\gamma$  Gaussian integrals. In general, the change of variables  $(\gamma - \mu)/\sigma \rightarrow \gamma$  simplifies the calculations. We obtain

$$M_{\mu\mu} = 1/(4\sqrt{\pi}\sigma^3), \quad M_{\sigma\sigma} = 3/(8\sqrt{\pi}\sigma^3), \quad M_{\mu\sigma} = M_{\sigma\mu} = 0$$

where the cross-term is null due to the odd-symmetry of the integrand function. The diagonal structure of this matrix simplifies the calculations considerably. The inverse matrix becomes

$$M_{kj}^{-1} = 4\sqrt{\pi}\sigma^3 \begin{bmatrix} 1 & 0 \\ 0 & 2/3 \end{bmatrix} \quad (\text{B 11})$$

For the column vector, we obtain

$$V_\mu = \frac{a(-2\mu^2 + \sigma^2)}{8\sqrt{\pi}\sigma^3} - \frac{b}{\sigma^3}(0.423142\mu^3 + 0.211571\mu\sigma^2)$$

$$V_\sigma = -\frac{3a\mu}{4\sqrt{\pi}\sigma^2} + b \left( -0.343803 + 0.105786\frac{\mu^4}{\sigma^4} - 0.95207\frac{\mu^2}{\sigma^2} \right)$$



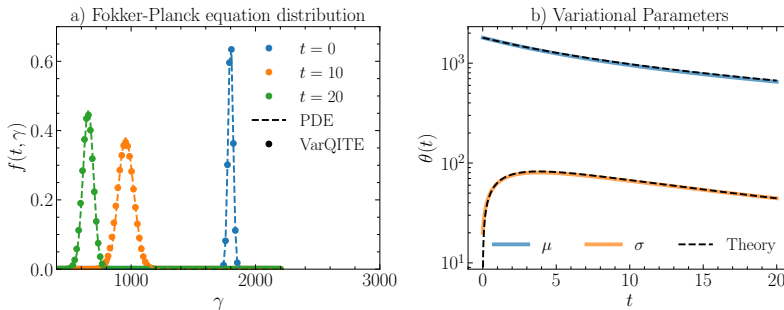


FIGURE 12. Numerical simulation of the Fokker-Planck equation with  $\chi_0 = 10^{-2}$ . a) The evolution of the distribution function  $f(t, \gamma)$ . The dashed line represents the result from a standard PDE solver, while circles represent the numerical integration of the MVP equations. b) The evolution of the moments. The colored lines represent the moments of the distribution function obtained from the PDE solver, while dashed lines represent the analytical results of equations 2.5 and 2.6.

Applying the inverse matrix  $M_{kj}^{-1}$  to the column vector  $V_k$ , we obtain

$$\begin{bmatrix} \dot{\mu} \\ \dot{\sigma} \end{bmatrix} = \begin{bmatrix} \underline{-a\mu^2 + 3b\mu^3 + 0.5a\sigma^2 + 1.5b\mu\sigma^2} \\ \underline{-2a\mu\sigma + b\mu^4/(2\sigma) - 4.5b\mu^2\sigma - 1.625\sigma^3b} \end{bmatrix} \quad (\text{B } 12)$$

Changing notation  $2\alpha_{rr} = a$  and  $b\mu^4 = B/(m^2c^2)$ , the underlined terms, which are leading order assuming  $\mu \gg \sigma$ , recover the results of equations 8 and 14 from the reference Vranic *et al.* (2016).

In figure 12, we show a comparison between a PDE solver solution of the Fokker-Planck equation, a numerical solution of the MVP equations using the ansatz B9 (without a quantum circuit), and the analytical solution 2.5. The numerical grid had  $2^7$  cells, the number of timesteps was 900 for a maximum simulation time of 20,  $\chi_0 = 10^{-2}$ , and initial momenta  $\mu_0 = 1800, \sigma_0 = 20$ .

We have thus shown the potential of MVP for retrieving the distribution moments in Quantum Radiation Reaction.

## REFERENCES

- ABRAMOWICZ, HALINA, ACOSTA, UWE HERNANDEZ, ALTARELLI, MASSIMO, ASSMANN, RALPH, BAI, ZHAOYU, BEHNKE, TIES, BENHAMMOU, YAN, BLACKBURN, THOMAS, BOOGERT, STEWART, BORYSOV, OLEKSANDR, BORYSOVA, MARYNA, BRINKMANN, REINHARD, BRUSCHI, MARCO, BURKART, FLORIAN, BÜSSER, KARSTEN, CAVANAGH, NIALL, DAVIDI, OZ, DECKING, WINFRIED, DOSSELLI, UMBERTO, ELKINA, NINA, FEDOTOV, ALEXANDER, FIRLEJ, MIROSLAW, FIUTOWSKI, TOMASZ, FLECK, KYLE, GOSTKIN, MIKHAIL, GROJEAN, CHRISTOPHE, HALLFORD, JOHN ANDREW, HARSH, HARSH, HARTIN, ANTHONY, HEINEMANN, BEATE, HEINZL, TOM, HELARY, LOUIS, HOFFMANN, MARIUS, HUANG, SHAN, HUANG, XINHE, IDZIK, MAREK, ILDEBERTON, ANTON, JACOBS, RUTH MAGDALENA, KAEMPFER, BURKHARD, KING, BEN, LAKHNO, HLIB, LEVANON, ASSAF, LEVY, AHARON, LEVY, ITAMAR, LIST, JENNY, LOHMANN, WOLFGANG, MA, TENG, MACLEOD, ALEXANDER JOHN, MALKA, VICTOR, MELONI, FEDERICO, MIRONOV, ARSENY, MORANDIN, MAURO, MORON, JAKUB, NEGODIN, EVGUENI, PEREZ, GILAD, POMERANTZ, ISHAY, POESCHL, ROMAN, PRASAD, RAJENDRA, QUERE, FABIEN, RINGWALD, ANDREAS, ROEDEL, CHRISTIAN, RYKOVANOV, SERGEY, SALGADO, FELIPE, SANTRA, ARKA, SARRI, GIANLUCA, SAEVERT, ALEXANDER, SBRIZZI, ANTONIO, SCHMITT, STEFAN, SCHRAMM, ULRICH, SCHUWALOW, SERGEJ, SEIPT, DANIEL, SHAIMERDENOVA, LEILA, SHCHEDROLOSIEV, MYKYTA, SKAKUNOV, MAKSIM, SOREQ, YOTAM, STREETER, MATTHEW, SWIENTEK, KRZYSZTOF, HOD, NOAM TAL,

- TANG, SUO, TETER, THOMAS, THODEN, DANIEL, TITOV, ALEXANDER, TOLBANOV, OLEG, TORGRIMSSON, GREGER, TYAZHEV, ANTON, WING, MATTHEW, ZANETTI, MARCO, ZARUBIN, ANDREI, ZEIL, KARL, ZEPF, MATT & ZHEMCHUKOV, ALEKSEY 2021 Conceptual Design Report for the LUXE Experiment. *The European Physical Journal Special Topics* **230** (11), 2445–2560, arXiv: 2102.02032.
- ABRAMOWICZ, H., ALTARELLI, M., ASSMANN, R., BEHNKE, T., BENHAMMOU, Y., BORYSOV, O., BORYSOVA, M., BRINKMANN, R., BURKART, F., BÜSSER, K., DAVIDI, O., DECKING, W., ELKINA, N., HARSH, H., HARTIN, A., HARTL, I., HEINEMANN, B., HEINZL, T., TALHOD, N., HOFFMANN, M., ILDERTON, A., KING, B., LEVY, A., LIST, J., MAIER, A. R., NEGODIN, E., PEREZ, G., POMERANTZ, I., RINGWALD, A., RÖDEL, C., SAIMPERT, M., SALGADO, F., SARRI, G., SAVORAY, I., TETER, T., WING, M. & ZEPF, M. 2019 Letter of Intent for the LUXE Experiment, arXiv: 1909.00860.
- ABRAMOWITZ, M. & STEGUN, I.A. 1964 *Handbook of Mathematical Functions with Formulas, Graphs, and Mathematical Tables. Applied Mathematics Series 0-486-61272-4*. U.S. Government Printing Office.
- ALGHASSI, HEDAYAT, DESHMUKH, AMOL, IBRAHIM, NOELLE, ROBLES, NICOLAS, WOERNER, STEFAN & ZOUFAL, CHRISTA 2022 A variational quantum algorithm for the Feynman-Kac formula. *Quantum* **6**, 730.
- AMARO, ÓSCAR & CRUZ, DIOGO 2023 A Living Review of Quantum Computing for Plasma Physics, arXiv: 2302.00001.
- ARTEMENKO, I. I., KRYGIN, M. S., SEREBRYAKOV, D. A., NERUSH, E. N. & KOSTYUKOV, I. YU 2019 Global constant field approximation for radiation reaction in collision of high-intensity laser pulse with electron beam. *Plasma Physics and Controlled Fusion* **61** (7), 074003.
- BERGHOLM, VILLE, IZAAC, JOSH, SCHULD, MARIA, GOGOLIN, CHRISTIAN, AHMED, SHAHNAWAZ, AJITH, VISHNU, ALAM, M. SOHAIB, ALONSO-LINAJE, GUILLERMO, AKASHNARAYANAN, B., ASADI, ALI, ARRAZOLA, JUAN MIGUEL, AZAD, UTKARSH, BANNING, SAM, BLANK, CARSTEN, BROMLEY, THOMAS R., CORDIER, BENJAMIN A., CERONI, JACK, DELGADO, ALAIN, MATTEO, OLIVIA DI, DUSKO, AMINTOR, GARG, TANYA, GUALA, DIEGO, HAYES, ANTHONY, HILL, RYAN, IJAZ, AROOSA, ISACSSON, THEODOR, ITTAH, DAVID, JAHANGIRI, SORAN, JAIN, PRATEEK, JIANG, EDWARD, KHANDLWAL, ANKIT, KOTTMANN, KORBINIAN, LANG, ROBERT A., LEE, CHRISTINA, LOKE, THOMAS, LOWE, ANGUS, MCKIERNAN, KERI, MEYER, JOHANNES JAKOB, MONTAÑEZ-BARRERA, J. A., MOYARD, ROMAIN, NIU, ZEYUE, O'RIORDAN, LEE JAMES, OUD, STEVEN, PANIGRAHI, ASHISH, PARK, CHAE-YEUN, POLATAJKO, DANIEL, QUESADA, NICOLÁS, ROBERTS, CHASE, SÁ, NAHUM, SCHOCH, ISIDOR, SHI, BORUN, SHU, SHULI, SIM, SUKIN, SINGH, ARSHPREET, STRANDBERG, INGRID, SONI, JAY, SZÁVA, ANTAL, THABET, SLIMANE, VARGAS-HERNÁNDEZ, RODRIGO A., VINCENT, TREVOR, VITUCCI, NICOLA, WEBER, MAURICE, WIERICHS, DAVID, WIERSEMA, ROELAND, WILLMANN, MORITZ, WONG, VINCENT, ZHANG, SHAOMING & KILLORAN, NATHAN 2022 PennyLane: Automatic differentiation of hybrid quantum-classical computations, arXiv: 1811.04968.
- BILBAO, P. J. & SILVA, L. O. 2023 Radiation Reaction Cooling as a Source of Anisotropic Momentum Distributions with Inverted Populations. *Physical Review Letters* **130** (16), 165101.
- BLACKBURN, T. G. 2024 Analytical solutions for quantum radiation reaction in high-intensity lasers. *Physical Review A* **109** (2), 022234.
- BONDARENCO, M. V. 2014 Multiphoton effects in coherent radiation spectra. *Physical Review D* **90** (1), 013019.
- BULANOV, S V, GRITANI, G M, SHAISULTANOV, R, ESIRKEPOV, T ZH, RIDGERS, C P, BULANOV, S S, RUSSELL, B K & THOMAS, A G R 2024 On the energy spectrum evolution of electrons undergoing radiation cooling. *Fundamental Plasma Physics* **9**, 100036.
- COLE, J. M., BEHM, K. T., GERSTMAYR, E., BLACKBURN, T. G., WOOD, J. C., BAIRD, C. D., DUFF, M. J., HARVEY, C., ILDERTON, A., JOGLEKAR, A. S., KRUSHELNICK, K., KUSCHEL, S., MARKLUND, M., MCKENNA, P., MURPHY, C. D., PODER, K., RIDGERS, C. P., SAMARIN, G. M., SARRI, G., SYMES, D. R., THOMAS, A. G. R., WARWICK, J., ZEPF, M., NAJMUDIN, Z. & MANGLES, S. P. D. 2018 Experimental Evidence of

- Radiation Reaction in the Collision of a High-Intensity Laser Pulse with a Laser-Wakefield Accelerated Electron Beam. *Physical Review X* **8** (1), 011020.
- CRUZ, FÁBIO, GRISMAYER, THOMAS, CHEN, ALEXANDER Y., SPITKOVSKY, ANATOLY & SILVA, LUIS O. 2021 Coherent Emission from QED Cascades in Pulsar Polar Caps. *The Astrophysical Journal Letters* **919** (1), L4.
- DASGUPTA, KALYAN & PAINE, BINOY 2022 Loading Probability Distributions in a Quantum circuit, arXiv: 2208.13372.
- DODIN, I. Y. & STARTSEV, E. A. 2021 On applications of quantum computing to plasma simulations. *Physics of Plasmas* **28** (9), 092101.
- ELI EXTREME LIGHT INFRASTRUCTURE <https://eli-laser.eu/>.
- ENDO, SUGURU, SUN, JINZHAO, LI, YING, BENJAMIN, SIMON C. & YUAN, XIAO 2020 Variational Quantum Simulation of General Processes. *Physical Review Letters* **125** (1), 010501.
- ENGEL, ALEXANDER, SMITH, GRAEME & PARKER, SCOTT E. 2019 Quantum algorithm for the Vlasov equation. *Physical Review A* **100** (6), 062315.
- FACET-II <https://facet-ii.slac.stanford.edu/facility>.
- FONSECA, R. A., SILVA, L. O., TSUNG, F. S., DECYK, V. K., LU, W., REN, C., MORI, W. B., DENG, S., LEE, S., KATSIOULEAS, T. & ADAM, J. C. 2002 OSIRIS: A Three-Dimensional, Fully Relativistic Particle in Cell Code for Modeling Plasma Based Accelerators. In *Computational Science — ICCS 2002* (ed. Peter M. A. Sloot, Alfons G. Hoekstra, C. J. Kenneth Tan & Jack J. Dongarra), *Lecture Notes in Computer Science* 978-3-540-47789-1, pp. 342–351. Berlin, Heidelberg: Springer.
- HARRIS, CHARLES R., MILLMAN, K. JARROD, VAN DER WALT, STÉFAN J., GOMMERS, RALF, VIRTANEN, PAULI, COUNAPEAU, DAVID, WIESER, ERIC, TAYLOR, JULIAN, BERG, SEBASTIAN, SMITH, NATHANIEL J., KERN, ROBERT, PICUS, MATTI, HOYER, STEPHAN, VAN KERKWIJK, MARTEN H., BRETT, MATTHEW, HALDANE, ALLAN, DEL RÍO, JAIME FERNÁNDEZ, WIEBE, MARK, PETERSON, PEARU, GÉRARD-MARCHANT, PIERRE, SHEPPARD, KEVIN, REDDY, TYLER, WECKESSER, WARREN, ABBASI, HAMEER, GOHLKE, CHRISTOPH & OLIPHANT, TRAVIS E. 2020 Array programming with NumPy. *Nature* **585** (7825), 357–362.
- HIBEF <https://www.hzdr.de/db/Cms?pOid=51491&pNid=711&pLang=en>.
- HIDALGO, LUIS & DRAPER, PATRICK 2024 Quantum simulations for strong-field QED. *Physical Review D* **109** (7), 076004.
- JAVADI-ABHARI, ALI, TREINISH, MATTHEW, KRSULICH, KEVIN, WOOD, CHRISTOPHER J., LISHMAN, JAKE, GACON, JULIEN, MARTIEL, SIMON, NATION, PAUL D., BISHOP, LEV S., CROSS, ANDREW W., JOHNSON, BLAKE R. & GAMBETTA, JAY M. 2024 Quantum computing with Qiskit, arXiv: 2405.08810.
- JIRKA, M., SASOROV, P., BULANOV, S. S., KORN, G., RUS, B. & BULANOV, S. V. 2021 Reaching high laser intensity by a radiating electron. *Physical Review A* **103** (5), 053114.
- JOSEPH, I., SHI, Y., PORTER, M. D., CASTELLI, A. R., GEYKO, V. I., GRAZIANI, F. R., LIBBY, S. B. & DUBOIS, J. L. 2023 Quantum computing for fusion energy science applications. *Physics of Plasmas* **30** (1), 010501.
- KHOKONOV, M. KH. 2004 Cascade processes of energy loss by emission of hard phonons. *Journal of Experimental and Theoretical Physics* **99** (4), 690–707.
- KOSTYUKOV, I. YU., NERUSH, E. N., MIRONOV, A. A. & FEDOTOV, A. M. 2023 Short-term evolution of electron wave packets in constant crossed electromagnetic fields with radiative corrections. *Physical Review D* **108** (9), 093007.
- KUBO, KENJI, NAKAGAWA, YUYA O., ENDO, SUGURU & NAGAYAMA, SHOTA 2021 Variational quantum simulations of stochastic differential equations. *Physical Review A* **103** (5), 052425.
- LOBET, M., D’HUMIÈRES, E., GRECH, M., RUYER, C., DAVOINE, X. & GREMILLET, L. 2016 Modeling of radiative and quantum electrodynamics effects in PIC simulations of ultra-relativistic laser-plasma interaction. *Journal of Physics: Conference Series* **688** (1), 012058.
- LOS, E. E., GERSTMAYR, E., ARRAN, C., STREETER, M. J. V., COLGAN, C., COBO, C. C., KETTLE, B., BLACKBURN, T. G., BOURGEOIS, N., CALVIN, L., CARDERELLI, J., CAVANAGH, N., DI PIAZZA, S. J. D. DANN A., FITZGARRALD, R., ILDERTON, A.,

- KEITEL, C. H., MARKLUND, M., MCKENNA, P., MURPHY, C. D., NAJMUDIN, Z., PARSONS, P., RAJEEV, P. P., SYMES, D. R., TAMBURINI, M., THOMAS, A. G. R., WOOD, J. C., ZEPF, M., SARRI, G., RIDGERS, C. P. & MANGLES, S. P. D. 2024 Observation of quantum effects on radiation reaction in strong fields, arXiv: 2407.12071.
- McLACHLAN, A.D. 1964 A variational solution of the time-dependent Schrodinger equation. *Molecular Physics* **8** (1), 39–44.
- MEDIN, ZACH & LAI, DONG 2010 Pair cascades in the magnetospheres of strongly magnetized neutron stars. *Monthly Notices of the Royal Astronomical Society* **406** (2), 1379–1404.
- MEUREN, SEBASTIAN, BUCKSBAUM, PHIL H., FISCH, NATHANIEL J., FIÚZA, FREDERICO, GLENZER, SIEGFRIED, HOGAN, MARK J., QU, KENAN, REIS, DAVID A., WHITE, GLEN & YAKIMENKO, VITALY 2020 On Seminal HEDP Research Opportunities Enabled by Colocating Multi-Petawatt Laser with High-Density Electron Beams, arXiv: 2002.10051.
- NEITZ, N. & DI PIAZZA, A. 2013 Stochasticity Effects in Quantum Radiation Reaction. *Physical Review Letters* **111** (5), 054802.
- NIEL, F., RICONDA, C., AMIRANOFF, F., DUCLOUS, R. & GRECH, M. 2018 From quantum to classical modeling of radiation reaction: A focus on stochasticity effects. *Physical Review E* **97** (4), 043209.
- NIELSEN, MICHAEL A. & CHUANG, ISAAC L. 2010 *Quantum Computation and Quantum Information: 10th Anniversary Edition*. Cambridge University Press.
- NSF-OPAL <https://www.lln.rochester.edu/index.php/omega-laser-facility-2/>.
- PAPADOPOULOS, D. N., ZOU, J. P., LE BLANC, C. & OTHERS 2016 The Apollon 10 PW laser: experimental and theoretical investigation of the temporal characteristics. *High Power Laser Science and Engineering* **4**, e34.
- PERUZZO, ALBERTO, McCLEAN, JARROD, SHADBOLT, PETER, YUNG, MAN-HONG, ZHOU, XIAO-QI, LOVE, PETER J., ASPURU-GUZI, ALÁN & O'BRIEN, JEREMY L. 2014 A variational eigenvalue solver on a photonic quantum processor. *Nature Communications* **5** (1), 4213.
- PODER, K., TAMBURINI, M., SARRI, G., DI PIAZZA, A., KUSCHEL, S., BAIRD, C. D., BEHM, K., BOHLEN, S., COLE, J. M., CORVAN, D. J., DUFF, M., GERSTMAYER, E., KEITEL, C. H., KRUSHELNICK, K., MANGLES, S. P. D., MCKENNA, P., MURPHY, C. D., NAJMUDIN, Z., RIDGERS, C. P., SAMARIN, G. M., SYMES, D. R., THOMAS, A. G. R., WARWICK, J. & ZEPF, M. 2018 Experimental Signatures of the Quantum Nature of Radiation Reaction in the Field of an Ultraintense Laser. *Physical Review X* **8** (3), 031004.
- PRESKILL, JOHN 2018 Quantum Computing in the NISQ era and beyond. *Quantum* **2**, 79.
- RIDGERS, C. P., BLACKBURN, T. G., SORBO, D. DEL, BRADLEY, L. E., SLADE-LOWTHER, C., BAIRD, C. D., MANGLES, S. P. D., MCKENNA, P., MARKLUND, M., MURPHY, C. D. & THOMAS, A. G. R. 2017 Signatures of quantum effects on radiation reaction in laser–electron-beam collisions. *Journal of Plasma Physics* **83** (5), 715830502.
- SATO, YUKI, KONDO, RUHO, HAMAMURA, IKKO, ONODERA, TAMIYA & YAMAMOTO, NAOKI 2024 Hamiltonian simulation for hyperbolic partial differential equations by scalable quantum circuits. *Physical Review Research* **6** (3), 033246.
- SCHOEFFLER, K M, GRISMAYER, T, UZDENSKY, D & SILVA, L O 2023 High-energy synchrotron flares powered by strongly radiative relativistic magnetic reconnection: 2D and 3D PIC simulations. *Monthly Notices of the Royal Astronomical Society* **523** (3), 3812–3839.
- SHEN, C. S. & WHITE, D. 1972 Energy Straggling and Radiation Reaction for Magnetic Bremsstrahlung. *Physical Review Letters* **28** (7), 455–459.
- SIM, SUKIN, JOHNSON, PETER D. & ASPURU-GUZI, ALAN 2019 Expressibility and entangling capability of parameterized quantum circuits for hybrid quantum-classical algorithms. *Advanced Quantum Technologies* **2** (12), 1900070, arXiv: 1905.10876.
- TIMOKHIN, A. N. 2010 Time-dependent pair cascades in magnetospheres of neutron stars – I. Dynamics of the polar cap cascade with no particle supply from the neutron star surface. *Monthly Notices of the Royal Astronomical Society* **408** (4), 2092–2114.
- TORGRIMSSON, GREGER 2024a Quantum radiation reaction: Analytical approximations and obtaining the spectrum from moments. *Physical Review D* **110** (7), 076012.

- TORGRIMSSON, GREGER 2024*b* Quantum radiation reaction spectrum of electrons in plane waves. *Physical Review D* **109** (7), 076030.
- UZDENSKY, DMITRI A. & RIGHTLEY, SHANE 2014 Plasma physics of extreme astrophysical environments. *Reports on Progress in Physics* **77** (3), 036902.
- VISSERS, GÉ & BOUTEN, LUC 2019 Implementing quantum stochastic differential equations on a quantum computer. *Quantum Information Processing* **18** (5), 152.
- VRANIC, MARIJA, GRISMAYER, THOMAS, FONSECA, RICARDO A. & SILVA, LUIS O. 2016 Quantum radiation reaction in head-on laser-electron beam interaction. *New Journal of Physics* **18** (7), 073035.
- XCELS <http://www.xcels.iapras.ru>.
- YOON, JIN WOO, JEON, CHEONHA, SHIN, JUNGHOON, LEE, SEONG KU, LEE, HWANG WOON, CHOI, IL WOO, KIM, HYUNG TAEK, SUNG, JAE HEE & NAM, CHANG HEE 2019 Achieving the laser intensity of  $5.5 \times 10^{22} \text{W/cm}^2$  with a wavefront-corrected multi-pw laser. *Opt. Express* **27** (15), 20412–20420.
- ZEUS <https://zeus.engin.umich.edu>.
- ZHANG, BO, ZHANG, ZHI-MENG & ZHOU, WEI-MIN 2023 Quantum splitting of electron peaks in ultra-strong fields. *Matter and Radiation at Extremes* **8** (5), 054003.